Bulletin of Engineering Geology and the Environment (2024) 83:71
https://doi.org/10.1007/s10064-024-03564-6

ORIGINAL PAPER

Numerical back analysis of an underground bulk mining operation using distributed optical fiber sensors for model calibration

Samuel Nowak[1] · Taghi Sherizadeh[1] · Mina Esmaeelpour[2] · Paul Brooks[3] · Dogukan Guner[1] · Kutay Karadeniz[1]

Received: 19 July 2023 / Accepted: 28 January 2024 / Published online: 10 February 2024

Abstract

Numerical modeling of complex underground engineering projects such as caverns, tunnels, and bulk mining zones is an essential part of the design phase. Large-scale models require significant reductions in complexity from the real-world scenario, which often leads to low confidence in the model output. In this work, a mine-scale numerical model is developed to simulate a room and pillar extraction mining operation. The model inputs are calibrated through the comparison of the model response to pillar extraction in an analogous mine geometry with measured strain values collected using a novel distributed optical fiber strain sensing technique after pillar extraction. Calibration efforts resulted in the identification of the extent of rock mass damage that resulted from the pillar extraction operation. Numerical model inputs were calibrated for geologic strength index (GSI), rock mass damage, discontinuity properties, and applied horizontal stress conditions. A range of calibrated model input parameters are provided, which show good correlation with measured field strain values and are shown to have an accuracy from 78.2 to 89.1% within a 50% tolerance interval of field data. The model calibration presented in this work represents the first step in a calibration process, from which the model will be used for the forward analysis of various mining scenarios, the results of which will inform future calibration and analysis.

Keywords Ground movement monitoring · Underground mining · Bulk mining · Ground control · Numerical model calibration · Geomechanics · Distributed optical fiber sensing

Introduction

Numerical models are powerful tools for the analysis of large engineering and mining projects in geomaterials and have been used extensively for the simulation of underground caverns, mine openings, and deep well bores. At large scales, geomaterials are notoriously heterogeneous, and their material properties may vary considerably from one area to another. A geomechanical assessment of a site area is reliant on the collection of data from the field via mapping, geophysics, and laboratory-scale mechanical testing. In order to use a numerical model for geomechanical analysis, the case must be simplified and idealized (Shapka-Fels and Elmo 2022). The wide range of material properties, spatial variation of geologic discontinuities and units, and the use of unverified assumptions in numerical modeling can lead to low confidence in the results of large-scale models. In addition, the inability to quantify the effect of engineering perturbations (such as rapid excavation, blasting, and undermining) often leads to over-simplification of complex problems.

Model calibration is the process of constraining numerical results with physical observations and measurements to gain confidence in the output of the model. Challenges arise in model calibration due to (1) the flexible constraints associated with data-poor and ill-understood complex natural systems, (2) the non-uniqueness of model outputs (in that multiple parameter input sets may result in the same outcome), and (3) limitations of available material models to describe the behavior of geomaterials (Walton and Sinha 2022). The associated limitations to model calibration often require an adaptive modeling approach in that insights into

✉ Taghi Sherizadeh
sherizadeh@mst.edu

[1] Department of Mining and Explosives Engineering, Missouri University of Science and Technology, Rolla, MO, USA

[2] Department of Electrical and Computer Engineering, Missouri University of Science and Technology, Rolla, MO, USA

[3] Nyrstar Tennessee Mines, Strawberry Plains, TN, USA

the physical system are developed and refined during the modeling process.

Physical observations for model calibration include measurement of the geomechanical response to some form of perturbation or changing condition (excavation, blasting, infiltration of water). Woo et al. (2012) used mine production data and Interferometric Synthetic Aperture Radar (InSAR) vertical displacement monitoring to calibrate a 32-Gm^3 model of a block caving mine. The model was calibrated using a back analysis procedure until a good correlation with InSAR data was achieved, thus allowing the calibrated model to be used with higher confidence and with accurate results for forward analysis (Woo et al. 2012). A cavity monitoring system (CMS) was used to quantify dilution occurring in underground stopes, which was used as a proxy for the developed zone of relaxation in numerical models for calibration (Cordova, et al. 2022). Instrumented cable bolts and convergence monitors were used to calibrate continuum and hybrid continuum-discontinuum models for a tunnel in jointed rock mass (Bahrani and Hadjigeorgiou 2018). Numerical model calibration can also be achieved using microseismic monitoring (Andrieux et al. 2008), empirical relationships (Esterhuizen et al. 2010), and laser mapping (Jones et al. 2016).

The ability of researchers to utilize monitoring data for the calibration of models pertaining to underground structures, however, is limited to the availability of monitoring instruments suitable for use underground, as technologies such as InSAR and laser mapping may be limited in applicability to the surface or near surface. In particular, laser mapping, while demonstrated to have significant applicability for measurement of surficial displacements in underground mine workings, has no ability to monitor within the rock mass, a critical gap for characterization of movement along discontinuity planes which may not daylight into the excavation. In addition, monitoring instruments available to the underground mining industry, such as borehole extensometers and crack meters, have severely limited ranges or installation depths, as well as high costs per sensor. These limitations result in the use of point-sensor data for the calibration of large and often geometrically complex underground structures. Distributed optical fiber sensing (DOFS) is a robust technology that offers potential solutions to address the drawbacks typically associated with point-sensing methods in underground rock structures. DOFS is the process of using an optical fiber as a modulator to changes in the environment around the fiber by converting quantities such as strain or temperature to changes in optical radiation (Gholamzadeh and Nabovati 2018). Brillouin optical time domain reflectometry (BOTDR) is a long-range (km scale) form of DOFS that has been deployed for strain measurement in oil and gas boreholes (Seabrook et al. 2022), tunnels (Moffat et al. 2015), and other underground caverns (Guan et al. 2015). Due to the meter-scale spatial resolution of most BOTDR systems, this technology has not been readily adopted by underground mining operations, as many mining applications for DOFS would involve cementing/grouting the fiber optic cable into boreholes, drilled into the rock, which would result in highly localized strains which are imperceptible to the BOTDR interrogation system. This limitation has been overcome with the development of the hybrid optical fiber cable (HOFC), which ensures a constant sensor gauge length even when installed in a brittle media (Nowak et al. 2022).

The use of DOFS via grouted boreholes allows for high-density sensor coverage over large underground areas, such as power caverns and bulk mining zones. Due to the low cost of optical fiber cable, installation of fiber optic networks is cost-effective and can provide exponentially more sensing points/dollar than many traditional borehole monitoring systems. In a recent study conducted by the authors of this paper, which is currently unpublished, a BOTDR sensing system integrating the HOFC was employed to monitor the progress of a pillar recovery operation within an underground metal mine. The data and field observations from this monitoring campaign form the basis for the calibration of a mine-scale numerical back analysis of the pillar extraction process. The resulting calibrated model can be used with higher confidence in its assumptions for forward analysis of future pillar recovery operations and support design. The results of the monitoring study and calibrated numerical model demonstrate the applicability of DOFS for mining applications and aid in the improvement of mining practices toward safer, more sustainable practices.

Young Mine case history

The Young Mine is an underground zinc mine located in the Mascot Jefferson City Zinc District (MJC), approximately 25 km northeast of Knoxville, TN (Fig. 1). The MJC has a rich mining history dating back to the 1880s, with three operational mines today which average 6000 tonnes per day.

Sphalerite ore deposits form as paleocarstic domal collapse breccias which are several kilometers in diameter. Domal breccias typically contain a low ore grade core, which consists of scantly mineralized or barren breccia. The host rock for the deposits consists of stratiform carbonate sedimentary rock packages, mainly comprised of dolostones with occasional thin shale beds. Structures such as bedding planes are shallowly dipping ($< 20°$) with good joint condition. Geologic strength index (GSI) values for the area fall between 59 and 75; however, in the site area specifically, the GSI values have been noted as high as 75 and not lower than 64.

The sphalerite ore is mined using the random room and pillar mining method, with pillar recovery when possible.

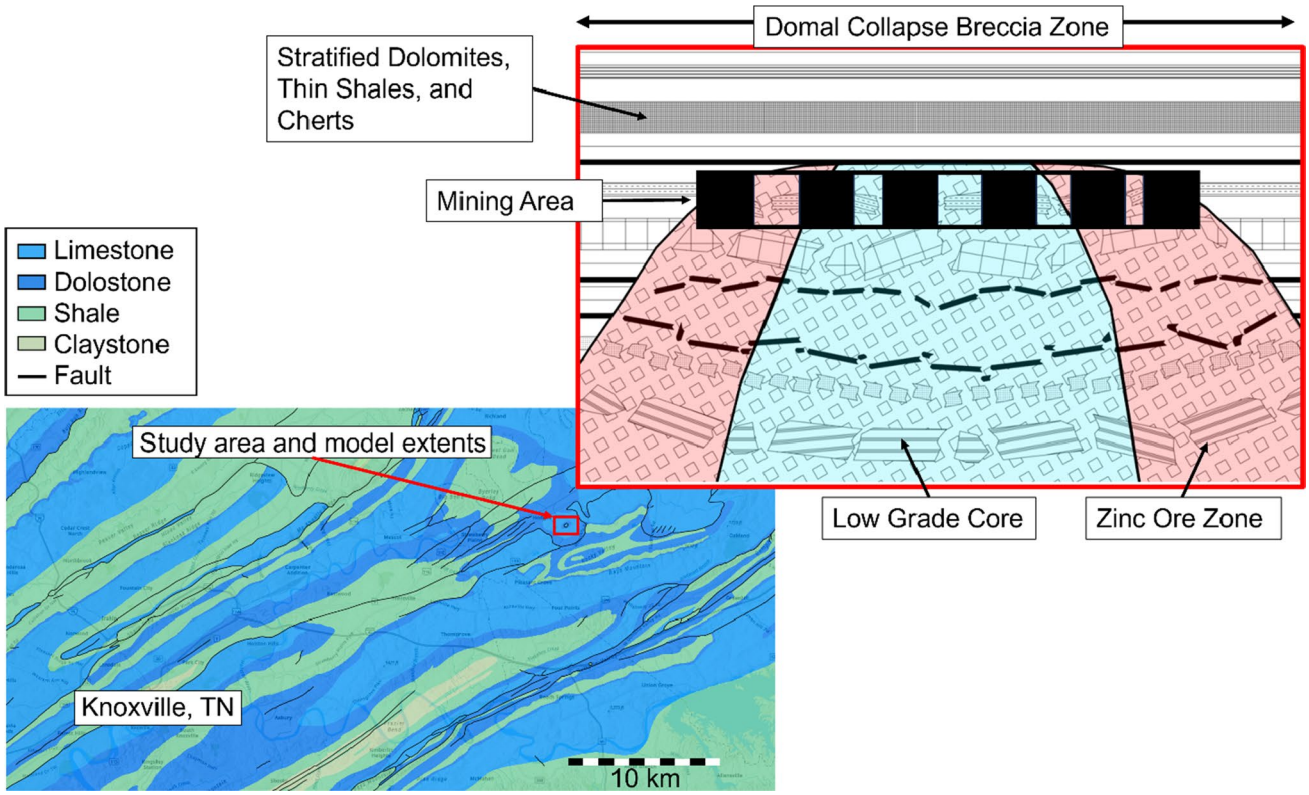

Fig. 1 Geologic map of Eastern Tennessee, with model extents and location denoted by the red box. The site area is comprised mainly of a paleocarstic domal collapse breccia (top right) surrounded by dolostone and occasional thin shale beds

A pillar extraction operation was monitored using the HOFC and a BOTDR interrogation system. A HOFC with a gauge length of 1.5 m was grouted into 12 boreholes with a max length of 22 m. Pillar extraction operations commenced several months after sensor installation, in which six large pillars were removed simultaneously (~ 3000 tonnes). Distributed strain measurements from the installed HOFC were made 2, 10, and 44 days after pillar extraction, at which point further excavation of the remaining pillars resulted in the total loss of the monitoring system. Removal of the pillars resulted in a failure of the roof in the stoping area up to a thin shale unit which was located approximately 10 m above the original roof line. In some areas within the stoping area, mainly the center where pillars were removed, failure 1–3 m beyond the thin shale unit was noted. The shale unit in question is a notable marker unit for the mine operator and one that has been noted to result in similar behaviors in other stoping areas, resulting in overbreak and dilution of the broken ore. The measurements collected from the DOFS monitoring system on the 44th day, as well as photographs taken after the pillar extraction are shown in Fig. 2. Failure past the primary support elements (2.1 m friction bolts) occurred almost immediately after pillar extraction, with ultimate failure up to the thin shale unit 10 m above the roof line occurring between the 10th and 44th days after pillar extraction.

Strain profiles from the near vertical boreholes show the highest observed extensional strain in the areas closest to the stope void, with measurements taken farther away from the stope void exhibiting strains with notably lower magnitudes. In the case of borehole 9, which is installed directly above the only remaining pillar in the stoping area, a large compressional strain was noted between the excavation roof and the thin shale bed, indicating that pillar extraction resulted in increased vertical loads transferred to the remaining pillar. It should be noted that compressional strains measured with DOFS indicate a slackening of the optical fiber. These strains are useful for determining strain regimes; however, the magnitude of compression may be erroneous.

The utilization of DOFS for strain monitoring in the room and pillar extraction operation presents a unique chance to calibrate numerical models effectively. This is made possible by the capability to collect a significant volume of high-precision strain data (measured at the με-level) from a single access point using cost-effective sensors. The data set collected in the presented monitoring study would likely have been cost-prohibitive using comparable instruments such as multi-point borehole extensometers. With low-cost sensors, larger monitoring

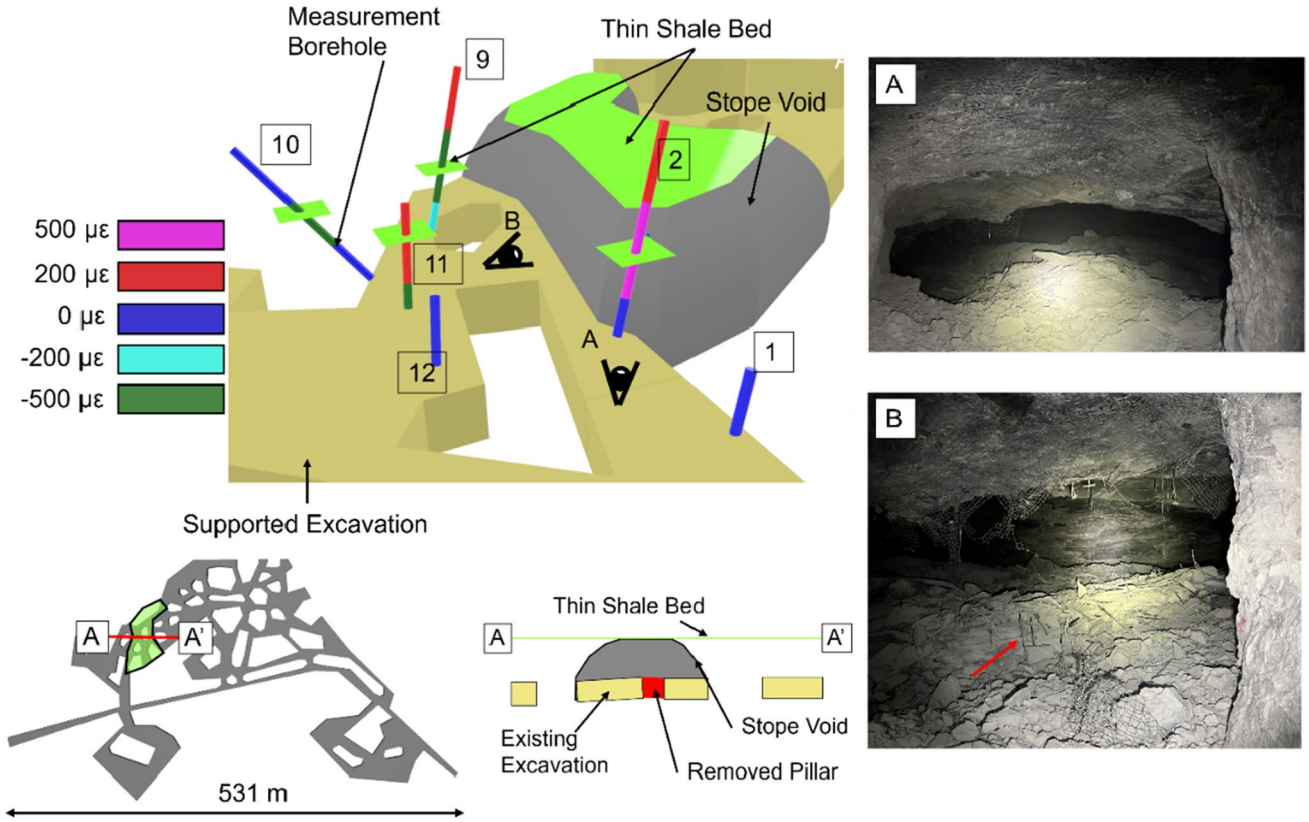

Fig. 2 (Left) Borehole traces colored by collected strain data using a BOTDR interrogation system on HOFC grouted into six boreholes (boxed numbers indicate borehole identification numbers) superimposed on a 3D excavation geometry of the pillar extraction area (stope void in gray) The location of the thin shale bed with respect to the stope void and borehole traces is shown in green. The plan view and cross-section of the area of interest are shown in the bottom left. (Right) Photographs of the stope void directly after pillar extraction. The red arrow points to failed friction bolts in the muck pile

data sets that cover entire mining areas are possible, leading to higher confidence in calibrated numerical model results.

Base model development

The study area is comprised mainly of bedded dolomites and is largely devoid of regular joint sets. Explicit modeling of each stratum across a mine-scale numerical model would result in a large number of numerical elements which would be computationally expensive to simulate. With the absence of intersecting joint planes, the use of continuum mechanics is a reasonable simplification for large-scale models. The rock mass at the site condition was treated as a continuum using FLAC3D version 7, with a single discontinuity plane (modeled as an interface) representing the thin shale bed that was encountered during the pillar extraction operation.

Young Mine 3D model geometry

The model geometry was developed from excavation surveys and geologic maps from the immediate study region. The model boundaries are located a minimum of 500 m from any excavation, with the exception of the model top, which represents the ground surface. A total model height of 550 m is utilized, with the center of the excavations located at a depth of 275 m. An analysis of stresses on the bottom layer of elements pre- and post-mining indicates minimal influence of excavation relaxation on the bottom boundary. The model is fixed in all directions on the bottom surface, with roller boundaries on all sides. The top of the model (ground surface approximation) is left unfixed. The excavation geometry represents the entire mining area, with the exception of some small access tunnels that lead from the modeled region outward. It is assumed that the overall impact of these tunnels on the area of interest is minimal. As a comparison of the model outputs with collected field data requires a high degree of geometrical twinning, care was taken to replicate

the geometry of the mine excavations, measurement boreholes, and geologic units/contacts as they appear in the field. Care was taken to ensure accuracy in geometry development (use of survey instruments for mapping of excavations and geologic contacts/units, use of multiple exposures/borehole televiewer in the mining area to ensure placement of geologic contacts), as well as in parameter inputs such as GSI measurements (collected and aggregated for several excavations in the areas from multiple personnel). The mine excavations and pillars are explicitly modeled as they appear in the field with slight simplifications in the general excavation profile to facilitate computations efficiently. The mine pillars to be removed as they were in the field are displayed in Fig. 3. Mapped geologic contacts and regional geologic information provided by the mine operator were used to inform the shape of the domal collapse breccia zone and low-grade core (Fig. 4). The thin shale unit is represented by a single interface located approximately 10 m vertically from the excavation roof. The interface extends through the entire model extents. Tetrahedral elements with a maximum edge length of 0.6 m are used within the area of interest and gradually increased in size to a maximum edge length of 75.0 m on the edges of the model. The fine mesh zone was assigned using a polyhedron with a 25-m horizontal buffer zone around the excavations, with a height of 50 m (10 m below the excavation floor and 40 above). The element size used in the area of interest was selected to be sufficiently smaller than the gauge length of the strain sensor used in the monitoring study (1.5 m). A total of 10e6 elements are required for the model geometry.

Rock mass properties

Initial estimates of rock mass properties for the three rock types are estimated from field observations and laboratory-scale mechanical testing of rock specimens. Lump samples collected at the room and pillar extraction site of the ore breccia and low-grade core barren breccia rock types, as well as drill core samples of dolostone, were tested in the uniaxial compression test and triaxial compression test according to ASTM standards (Standard ASTM 2014). Indirect tensile (Brazilian disc) tests were conducted (Standard ASTM 2016) to obtain intact tensile strength values. The results of the uniaxial and triaxial compression tests (Fig. 5) indicate that there is not a large variation in rock stiffness or strength between the three rock types tested, and mostly brittle failure was observed. The failure states of triaxial and uniaxial compression tests were used to fit a Hoek–Brown failure envelope to the data. The values of m_i for breccia and dolomite were assumed from RocScience (2023). Intact rock parameters obtained from laboratory testing are presented in Table 1.

Field mapping at the site and on surface outcrops nearby indicate that a range of GSI in the study region

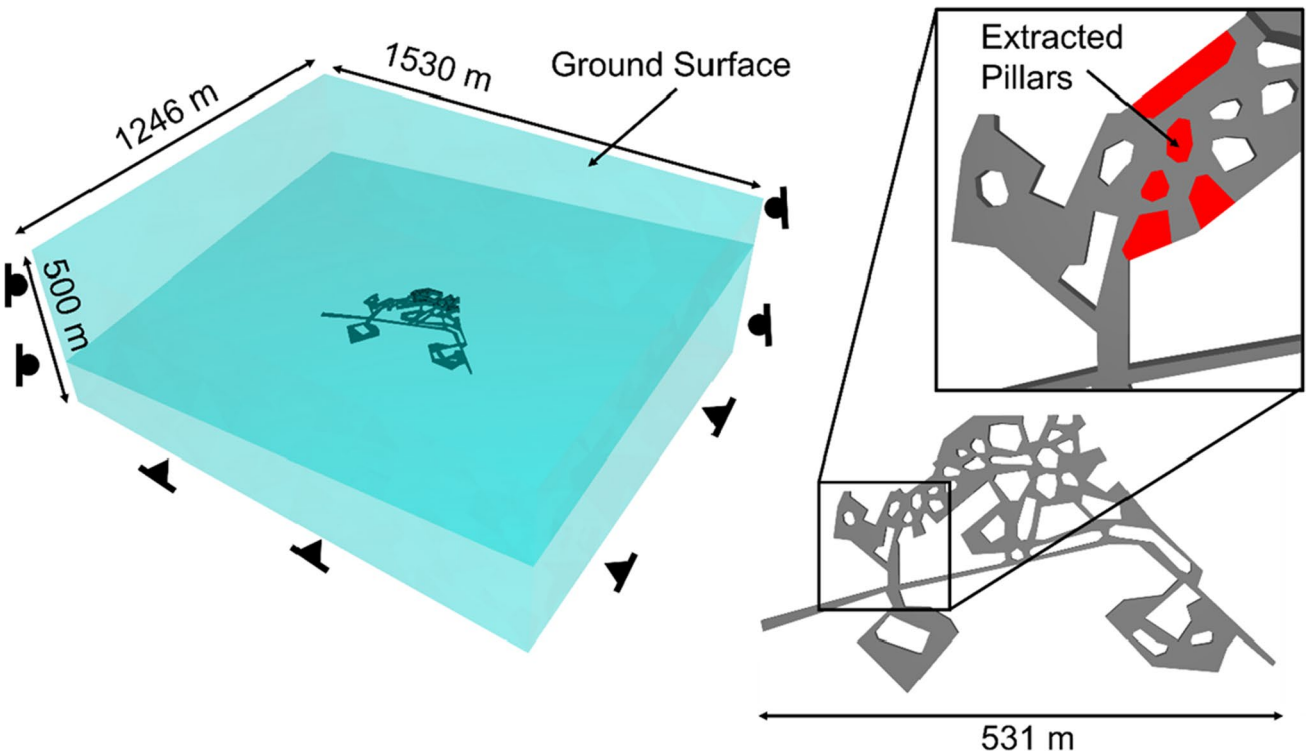

Fig. 3 Model extents and excavation geometry

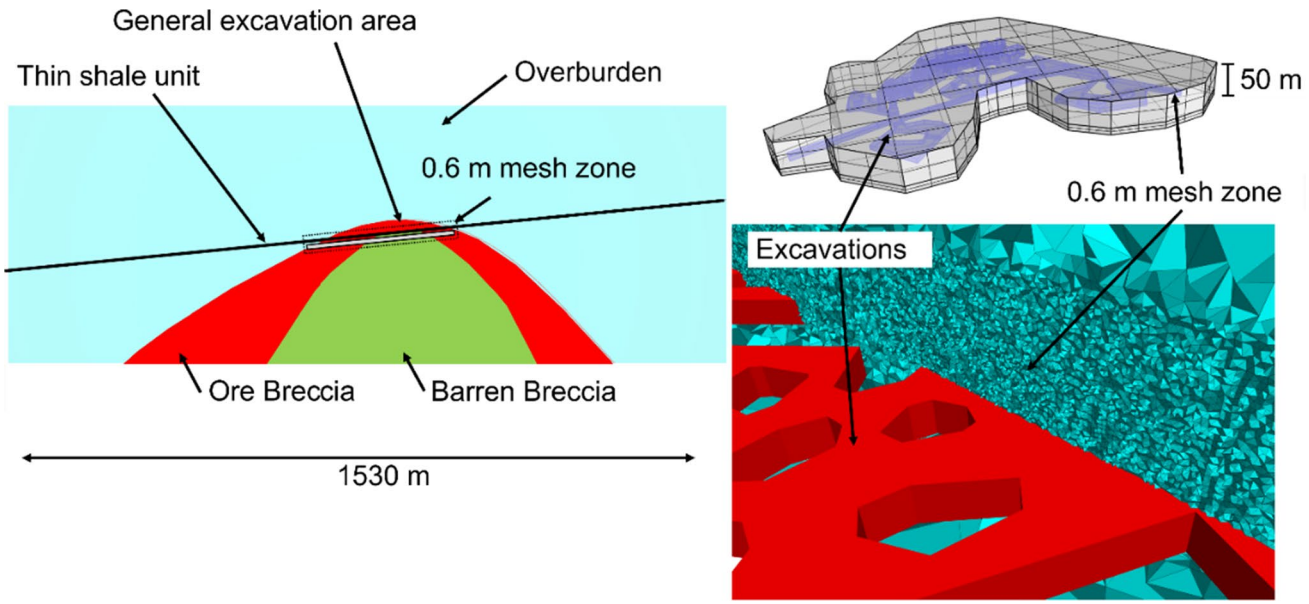

Fig. 4 (Left) Cross-section of model showing the location of the general excavation area, the thin shale bed, and the paleocarstic domal collapse breccias. (Top right) Polyhedron is used to assign the fine mesh zone around the excavation area. (Bottom right) The clipped cross-section of the model shows mesh size gradation from the 0.6-m fine mesh zone to the coarse 75-m mesh on the boundaries

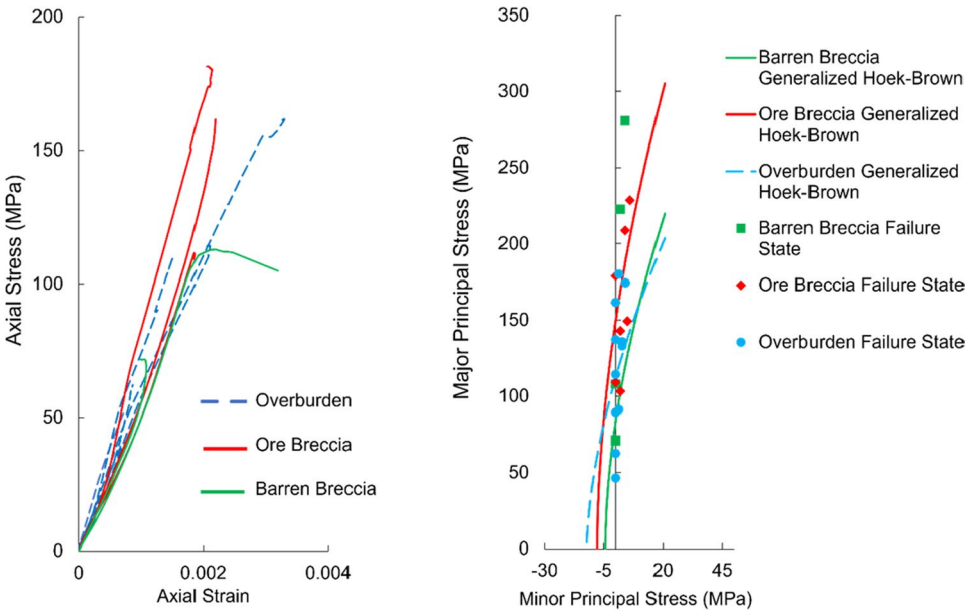

Fig. 5 Intact rock test results. (Left) Uniaxial compression test stress–strain curves for the three rock types tested. (Right) Hoek–Brown failure criteria fitted to triaxial compression test results

Table 1 Intact rock properties and rock mass properties

Intact rock properties						Rock mass strength properties				
Rock type	Bulk modulus (GPa)	Shear modulus (GPa)	m_i	σ_T(MPa)	UCS (MPa)	GSI	$\sigma_{T_{rm}}$(MPa)	a	s	m_b
Barren breccia	35.2	34.0	19	−4.45	84.65	60–75	0.21–0.66	0.501–0.503	0.0117–0.0622	4.55–7.78
Ore breccia	26.5	24.0	19	−7.25	137.75	60–75	0.38–1.19	0.501–0.503	0.0117–0.0622	4.55–7.78
Overburden	47.8	25.5	9	−4.31	112.26	60–75	0.61–1.89	0.501–0.503	0.0117–0.0622	2.16–3.69

ranges between 60 and 75. Specifically, in the room and pillar extraction area, GSI values were noted to be closer to the upper end of this range. The generalized Hoek–Brown (Hoek and Brown 2019) criterion was used to adjust the intact rock parameters to the rock mass scale. A disturbance factor of $D = 0.0$ is utilized in the model for non-excavation areas. In development headings, blasting practices at the mine site are generally good, with occasional minor overbreaks occurring in normal mining conditions. A borehole camera was used to assess fracturing into the rock in areas excavated for development; however, no notable features were identified. Rock mass damage in development headings and production (room and pillar extraction) stopes is addressed in the "Damage zone" section. RSData software was used to convert laboratory scale triaxial tests to rock mass parameters (Table 1).

Competent rock mass has often been noted to exhibit similar elastic moduli to laboratory scale specimens, such as described in Kellaway and Keyter (2012), where intact moduli were assigned to competent mudstones with the assumption of lowered GSI values. Jointing at the study area is minimal, with typical spacing between joints of more than 2 m. The bulk and shear modulus assigned to the numerical model are that of the average estimates from the laboratory scale testing.

Support elements

Ground support at the study area is accomplished with 2.1-m friction bolts on a 1.2 m × 1.2 m pattern across the excavation roof. This support system is modeled explicitly in FLAC3D using the hybrid bolt command. Support elements are installed with the same spacing and length as in the study area (Fig. 6).

The pull-out test results were provided by the mine operator, which served as a basis for the calibration of structural elements in the developed model. A simplified model was constructed to replicate the pull-out test in FLAC3D. The simplified model consists of a 2.1 m by 0.5 m 0.5 m block of rock with material properties consistent with middling values of ore breccia, which forms the immediate roof in much of the site area. In situ stresses are applied according to those discussed in the "Stress initialization and excavation sequence" section. FLAC3D hybrid structural elements were used, and the parameters changed until a good correlation between the experimental and numerical results was achieved (Fig. 7). No post-failure behavior is expected, and an average pull-out strength of 68.8 kN with a displacement of 25.4 mm was noted in the field.

The support element calibration yielded a set of structural element properties which were used in all subsequent modeling efforts (Table 2):

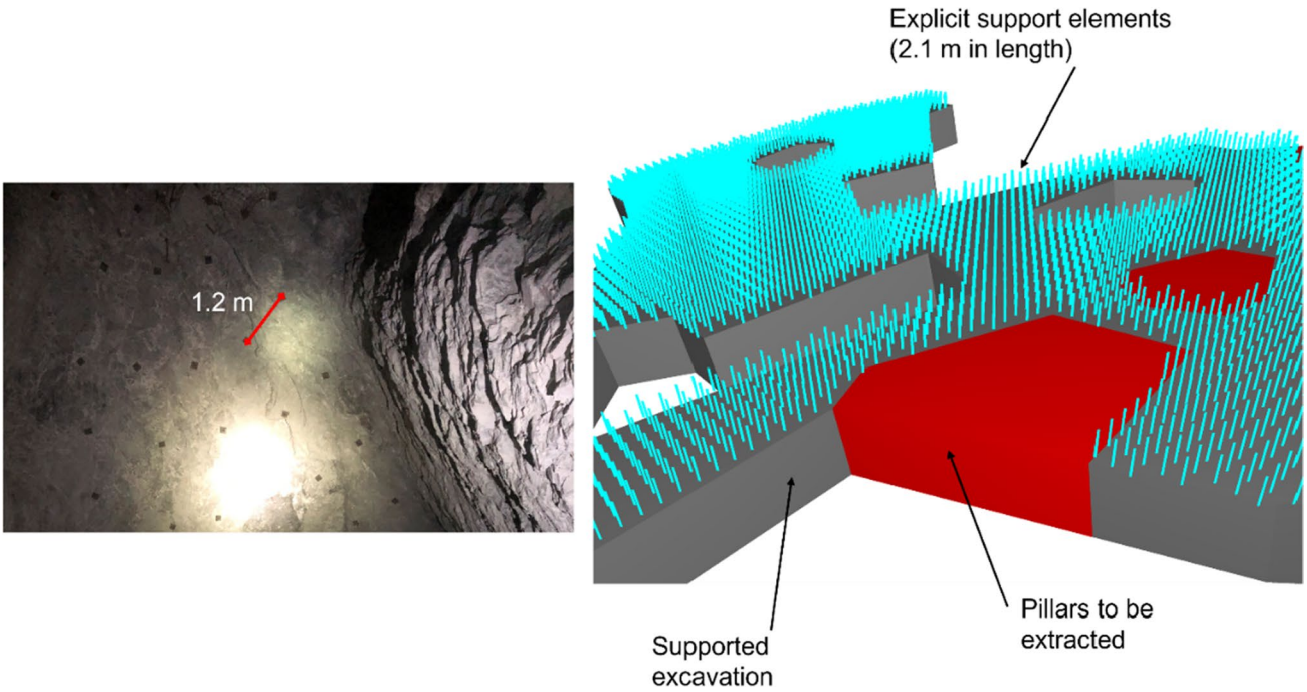

Fig. 6 (Left) Friction bolts installed in pillar extraction area on a roughly 1.2 m × 1.2 m spacing. (Right) Explicit hybrid support elements modeled in FLAC3D

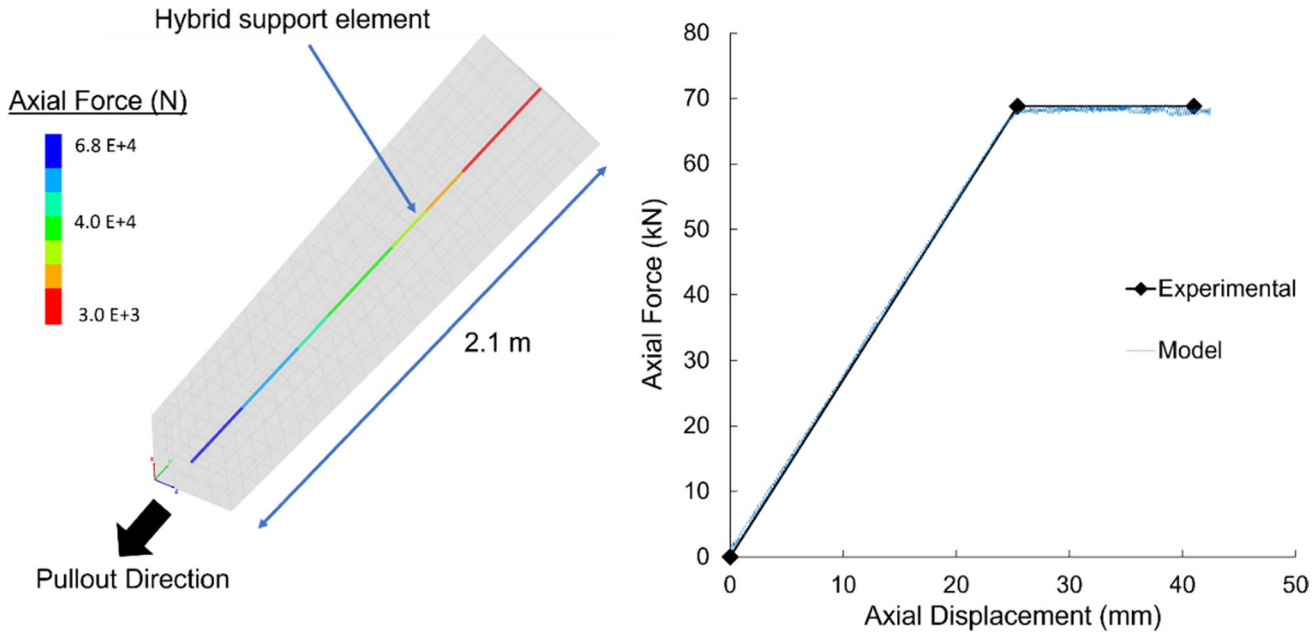

Fig. 7 Calibration of structural elements, (left) pull-out test model in FLAC3D, (right) comparison of numerical pull-out tests with experimental results

Table 2 Calibrated structural element support parameters

Property	Value	Unit
Cross-sectional area	478	mm^2
Young's modulus	80	GPa
Grout stiffness	1.35	MPa/m
Grout cohesion	3.2	kPa
Yield tension	35.4	kPa
Tensile failure strain	0.207	
Dowel active length	7.0	mm
Dowel stiffness	3.5	MPa
Dowel yield	19.9	kPa
Dowel failure strain	0.8	

Stress initialization and excavation sequence

Young Mine is located near Knoxville, TN, near the Appalachian Ridge and Valley physiogeographic region. This area is characterized as an oblique-normal to strike-slip tectonic regime (Levandowski et al. 2018). Vertical stresses are considered to be a principal stress in the Appalachian region (Bowersox et al. 2021), and an initial value of maximum horizontal stress of 1.25 σ_v for the oblique-normal regime. The mine operator has indicated in conversation that institutional or legacy knowledge of maximum horizontal stresses for the site yields estimates as high as 2.0 σ_v. The direction of maximum horizontal principal stress has been estimated regionally by borehole breakout testing to be N53° E (Bowersox et al. 2021). As few formal stress measurements have been made in the site area, in situ stresses are among the parameters that will be investigated during the calibration phase.

Underground hard rock mining using the drill and blast method often results in a span of time between excavation and installation of primary roof support. To simulate this effect, rock bolt installation and tunnel excavation in the base model are accomplished by partial sequential excavation, support installation, and full sequential excavation. Excavation of the main tunnels was accomplished in the model using the zone relax logic. The main excavations or development tunnels were excavated in the model in 16 even segments, the sequence of which was determined from production data provided by the mine operator. For each main excavation segment in the sequence, the following procedure was followed: (1) relax the elements within the excavation group by 30% (accomplished by multiplying the material properties assigned to those elements by a factor of 0.7), (2) install rock bolts in the region of the relaxed excavation, and (3) fully relax the excavation. Zone relaxation was conducted over a total of 5000 model steps for each excavation, with a uniform 1500 steps per every 10% of the total relaxation. This relaxation routine was selected after a comparison between zone failure states at the edges of the excavations for a range of relaxation steps. The authors noted that the selected relaxation routine (1500 steps per 10% total relaxation) yielded results similar to those observed in the excavations at the mine site, such as minimal damage zones

in development headings. At the conclusion of the sequential excavation process, the pillar extraction process began. In the field, all mine pillars were removed simultaneously in one large production blast. This effect was replicated in the model using the zone relax logic to 100% without the addition of support elements over a 5000-model step period. At the conclusion of pillar extraction, the model was allowed to run until a global unbalanced force ratio of $1e-5$ was achieved. The global unbalanced force was used to ensure that small instabilities did not result in untenable model run times. The entire model process requires 3 days of run-time on a computer with middling performance.

Model calibration

Through the explicit modeling of the complex mine geometry, measured strain values from field monitoring are compared with the numerical model predicted values. The latest available data from the DOFS monitoring system (44 days after pillar extraction) was utilized for model calibration. The mine operator required 44 days after pillar extraction to access the stoping area for collection of broken ore and setup of the next round of pillar extraction; thus, the numerical models can be considered calibrated for the timescale in which the excavation would be utilized. Model outputs are collected in the form of total strain profiles, the locations of which in the model correspond with the measurement boreholes used for DOFS installation in the active mine site. For model calibration, DOFS data was considered a series of individual point sensors in a line, with the distance between centers taken as the gauge length of the HOFC (1.5 m). As only extensional strain magnitudes can be quantified using the HOFC, areas in which compressional strain values were noted were omitted from the calibration data set. Due to the complexity of the mine geometry and uncertainty in the exact location of measurement boreholes, model output data that falls within 50% of the measured strain values ($\pm$ the 120 με noise level of the BOTDR interrogation system) are considered acceptable.

An initial sensitivity analysis was conducted to ensure that model outputs would be within an acceptable range of the measured field data. The initial sensitivity analysis was conducted with rock mass parameters ranging from a GSI of 80 to 55 and maximum horizontal stresses ranging from 0.5 to 2.0. From this initial analysis, it was found that model outputs for GSI values at the extreme ends of the range (80 and 55) produced model strain values that exhibited smaller or larger than expected from the field data, respectively. In addition, it was found that minimum and maximum horizontal stress values of $0.75\sigma_v$ and $1.25\sigma_v$ produced initial model outputs that most closely matched those of the field data.

An analysis of borehole scope data from the active mine site yielded little to no evidence of blast damage into the rock from normal development blasting. This lack of evidence suggests that an initial value of $D=0.0$ may be applicable to all development areas within the active mine site. This assumption, however, does not pertain to production blasting areas, in which much higher powder factors are used, and large open areas between pillars may act to channel excess blast energy into the surrounding rock. In order to quantify the extent and magnitude of the blast damage zone that results from the pillar extraction process, the initial calibration process was conducted with a damage factor of $D=0.0$ to be updated upon analysis of the model results in comparison to field data.

A parametric analysis of a large number of parameters, each with a range of possible values, is often not possible when using a factorial experimental design when computational run times are long. Taguchi experimental design is the process of using orthogonal arrays to test pairs of parameters simultaneously, thus reducing overall computational time (Taguchi and Phadke 1984). This has been experimented extensively by Kim et al. (2018) for calibration of coal mine models. For the calibration of the mine scale numerical model, a set of parameters was chosen that reflect the properties of the rock mass itself, and the thin shale bed in the immediate roof section. A total of five parameters, each with four levels that represent the possible ranges, were selected (Table 3). When combined in an orthogonal array via the Taguchi method, a total of 16 numerical model runs are required to test all necessary combinations (Table 4). The Taguchi method allows for the rapid identification of parameters with the highest impact on model output and thus allows researchers to identify candidate parameters for further analysis.

Model outputs take the form of total strain profiles from modeled regions which correspond to the location of

Table 3 Parametric ranges used in the Taguchi experimental design

Parameter	Level 1	Level 2	Level 3	Level 4
Geologic strength index (GSI, $D=0.0$)	75	70	65	60
Joint stiffness: normal/shear (GPa/m)	20.0/0.2	15.0/1.5	5.0/0.5	1.0/0.1
Joint cohesion (Pa)	1e6	1e5	1e4	0.0
Joint tension (Pa)	1e4	1e3	1e2	0
Joint friction angle (°)	21	14	7	0

Table 4 Taguchi orthogonal array used for initial model calibration

Model observation	Geologic strength index (GSI, $D=0.0$)	Joint stiffness: normal/shear (GPa/m)	Joint cohesion (Pa)	Joint tension (Pa)	Joint friction angle (°)
OBS1	75	20/0.2	1e6	1e4	21
OBS2	75	15/1.5	1e5	1e3	14
OBS3	75	5/0.5	1e4	1e2	7
OBS4	75	1/0.1	0	0	0
OBS5	70	20/0.2	1e5	1e2	0
OBS6	70	15/1.5	1e6	0	7
OBS7	70	5/0.5	0	1e4	14
OBS8	70	1/0.1	1e4	1e3	21
OBS9	65	20/0.2	1e4	0	14
OBS10	65	15/1.5	0	1e2	21
OBS11	65	5/0.5	1e6	1e3	0
OBS12	65	1/0.1	1e5	1e4	7
OBS13	60	20/0.2	0	1e3	7
OBS14	60	15/1.5	1e4	1e4	0
OBS15	60	5/0.5	1e5	0	21
OBS16	60	1/0.1	1e6	1e2	14

measurement boreholes installed at the active mine site. Measured data from the DOFS monitoring system is compiled, with the omission of strain data from compressional zones (negative strain values), from which the measured strain magnitudes are not applicable. Model outputs are compared to field data through plots of measured strain data versus model output total strain.

Due to the wide variety of numerical modeling methods and calibration routines, there is no available standard methodology for developing criteria for acceptable model outputs with respect to field data. Many studies presented in the literature show an ability to calibrate large numerical models to field data in small displacement zones but often report deviations from field data in higher displacement areas (those with close proximity to large excavations or tunnel boundaries). This issue is often exacerbated in studies that make use of large data sets or multiple instrumentation sites. A study utilizing four extensometers in a room and pillar mining operation produced a good correlation between field data and model outputs but noted that the developed model tended to overpredict displacement by more than 100% of measured field data in one measurement point (Walton et al. 2016). A similar discrepancy was reported in a 2D model of a tunnel monitored by several extensometers (Rafiei Renani et al. 2016). Model calibration criteria were developed for this study from an assessment of available literature, past experience, and engineering judgment. Given the complex geometry and large data set and the high precision of the DOFS measurements, model outputs that fall within ± 50% of the measured values (± the 120 με noise level of the BOTDR interrogation unit) are considered acceptable for calibration at this stage. This criteria was followed for the duration of the calibration process. The results of the Taguchi model calibration experiment are displayed in Fig. 8.

The initial model calibration indicates that GSI values above 70 and below 65 are likely to produce model results which under or over-predict rock mass strains with respect to measured field data, respectively. In addition, with the exception of the extreme case of models assigned a GSI of 60, interface parameters were found to have little influence on the model accuracy.

Reports from the mine operator indicate that a higher than usual powder factor was used for the pillar extraction operation to ensure ease of ore removal by remote-controlled equipment. The DOFS monitoring system consists of six boreholes, ranging in distance to the stope void from 6 to 30 m. With this range of measurement points, the location of the blast damage zone could be identified by comparing the model outputs to sensor data, identifying the zones in which the models correspond when no damage factor is assigned ($D=0$), and identifying the zones in which the model output under-predicts the deformation as those zones in which blast damage has occurred. There is a clear alignment of model outputs with measured data from boreholes 1, 10, and 12, with a departure from measured data from boreholes 2, 9, and 11 (the boreholes with the closest proximity to the stope void and highest recorded strain values, dotted oval on Fig. 8).

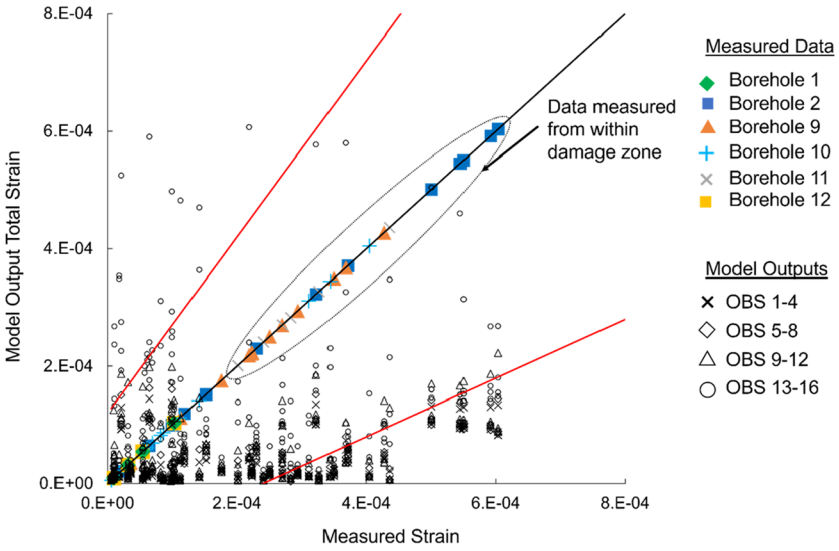

Fig. 8 Results of the Taguchi model calibration. The dotted circle encompasses measured data that was not accurately predicted by the model outputs. The area between red lines indicates an acceptable model accuracy zone (measured field values ± 50% of their value)

Damage zone

The initial model calibration in which a global damage factor of $D = 0.0$ was applied allows for the identification of the extent of the blast damage zone, which results from large bulk blasting practices. A shell polygon was constructed, encompassing the pillar extraction area and measurement borehole sites that correspond to modeled areas with low fidelity (lower than expected total strain values) to the measured data. The general shape of the shell polygon was informed by measured strain values, excavation geometry, and field observations of post-blasting conditions in the stope void. Polygons were constructed with increasingly smaller diameters to represent the increasingly localized blast damage zones, where the highest damage factor ($D = 1.0$) is assigned to zones within the inner-most shell. The damage factor was reduced for each successive shell until a value of $D = 0.2$ for the largest outer shell (Fig. 9).

The material properties of elements within the damage zone were degraded using the generalized Hoek Brown

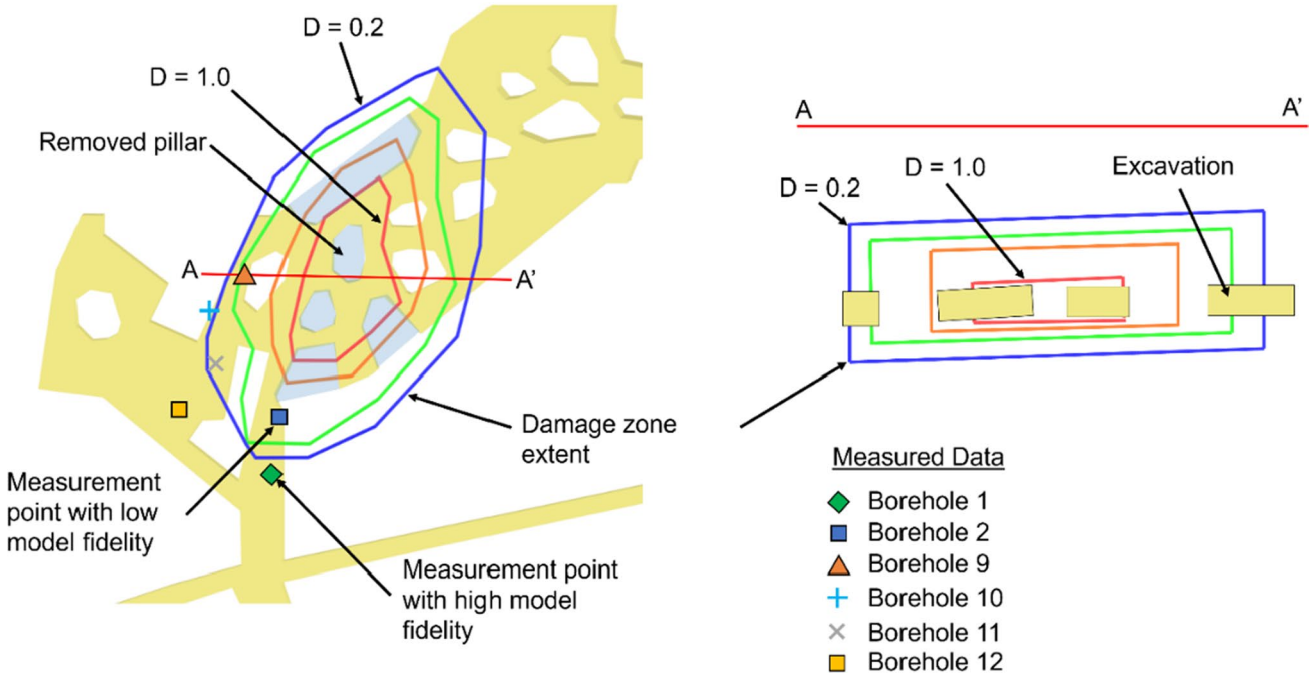

Fig. 9 Damage zones applied to modeled zones with low fidelity (lower than expected total strain values) to measured data. (Left) Plan view of damage zones with the locations of measurement borehole collars. (Right) Cross-section of damage zones through like A-A'

(Hoek and Brown 2019) directly after the removal of the pillars to simulate the onset of blast damage. The damage zone occurs entirely within the ore zone. Thus, only this rock type must be degraded, and there are no interactions between multiple damaged rock types. The rock mass parameters m_b and s are degraded via the damage factor using the method developed in Hoek (1994). The damaged rock mass properties assigned to zones within the damage zone for the two GSI values found to produce model outputs closest to measured field data in the initial calibration (GSI = 65 and 70) are presented in Table 5:

The applied damage zone increased model accuracy considerably. For example, a model with a GSI of 70 and no damage zone is compared to its damaged counterpart (Fig. 10). The model accuracy, calculated by comparing the number of data points that plot within the accepted tolerance ranges, was increased from 70.9 to 87.2%. The model result displayed in Fig. 10 still considerably under-predicts the high magnitude strain values from within the damage zone; thus, further calibration is required.

Table 5 Damaged rock mass properties assigned to zones within the damage zone

Rock type	GSI	D	s	m_b
Ore breccia	70	0.0	0.035674	6.51
Ore breccia	70	0.2	0.028116	5.78
Ore breccia	70	0.5	0.018316	4.55
Ore breccia	70	0.7	0.012935	3.65
Ore breccia	70	1.0	0.006738	2.23
Ore breccia	65	0.0	0.020468	5.44
Ore breccia	65	0.2	0.015504	4.74
Ore breccia	65	0.5	0.009404	3.59
Ore breccia	65	0.7	0.006267	2.78
Ore breccia	65	1.0	0.002928	1.56

Stress conditions

The study area is located within a tectonically complex region within the Appalachian Valley and Ridge province, with few available stress measurements. In addition, local paleocarstic domal collapse features, regional to local faulting, and a long history of bulk mining activity can also play a major role in determining in situ and induced stress conditions.

While the addition of the damage zone around the stoping area produced higher model accuracy, a discrepancy between higher measured strain values and model outputs indicated that accuracy could be improved considerably. Several models in which the damage zone was increased in magnitude (via increasing the size of the $D = 1.0$ shell) were examined; however, the general result was an increase in strain beyond acceptable limits in the low-strain areas (boreholes 1, 10, and 12). This result indicates that the initial assumptions on in situ stress magnitudes and the direction of maximum horizontal stresses may require further calibration. For horizontal stress calibration (both orientation and magnitude), a base model with a GSI of 70 and middling interface properties was utilized.

Vertical stresses in the study area are assumed to be a principal stress, and the location of the room and pillar extraction stope at the top of the dome feature would suggest that this is a reasonable assumption, as stresses are likely to be rotated tangentially to the dome surface. Horizontal stress directions were examined at 15° increments from the middling value used in the initial model calibration (N53° E), with a horizontal stress ratio of $0.75\sigma_v$ and $1.25\sigma_v$. The results (Fig. 11) indicate that the horizontal stress direction assigned at the model outset has little impact on the model fidelity to measured strain values.

The orientation of the maximum horizontal stress was then fixed at N53° E, and several horizontal stress magnitudes were examined. Legacy information at the mine site

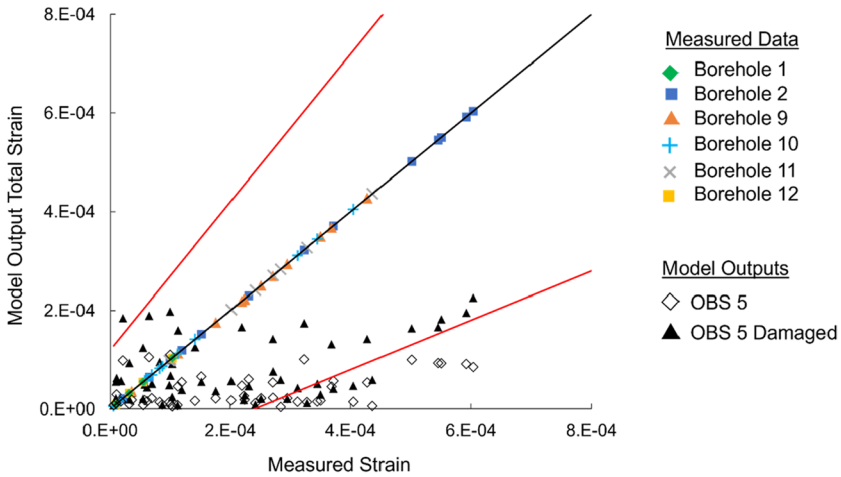

Fig. 10 The results of initial calibration for rock mass damage

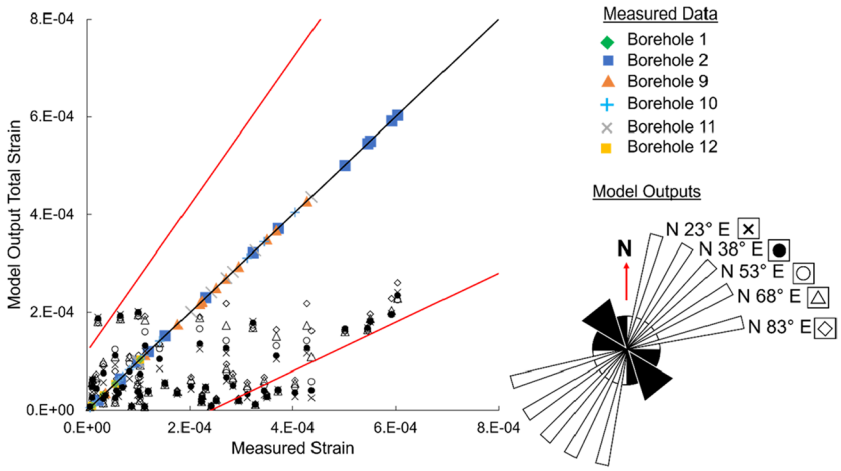

Fig. 11 Model calibration with respect to the direction of maximum horizontal stress

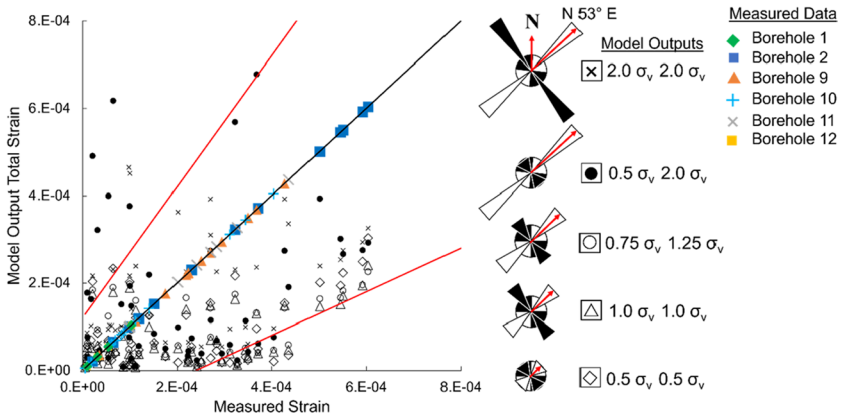

Fig. 12 Model calibration with respect to horizontal stress magnitudes

indicates that horizontal stresses can reach up to $2.0\sigma_v$; thus, several magnitudes were selected in which this was the maximum value examined. Several combinations of horizontal stresses are examined to identify the role of confining and deviatoric stresses on model accuracy.

The results of the stress magnitude calibration (Fig. 12) indicate that highly competent rock (GSI 70) under high confining stresses ($2.0\sigma_v$) results in a model output that matches measured data with 89.1% accuracy within the 50% tolerance interval.

Model calibration results

Using insights from the conducted modeling study, several responsive parameters are selected and combined to produce a range of parametric scenarios which result in more accurate model outputs with respect to measured field data. The initial model calibration (Fig. 8) indicates that GSI is likely the dominant controlling parameter in the model and that GSI values between 65 and 70 produce the most responsive model outputs, with higher or lower values resulting in excessive output deviations from field data. Calibration for stress conditions indicates that high horizontal stresses can result in more accurate model outputs when rock quality is high (GSI 70). Three condition scenarios are presented which represent the ranges of calibrated model parameters that result in the highest model accuracy (Table 6), the results of which are presented in Fig. 13.

Table 6 Three model scenarios that represent the highest model accuracy

Observation	GSI	Maximum horizontal stress	Horizontal stress min
OBS 17	65	$1.25\sigma_v$	$0.75\sigma_v$
OBS 18	70	$1.25\sigma_v$	$0.75\sigma_v$
OBS 19	70	$2\sigma_v$	$2\sigma_v$

A representative cross-section through the pillar extraction area (section line corresponds with that in Fig. 14) demonstrates that all three models produce similar failure patterns with those observed in the field, in which the roof of the pillar extraction area collapsed up to and in some areas beyond the thin shale bed. High strains and shear failures are noted in the remaining pillars, while tensile failures dominate the roof area above the removed pillars.

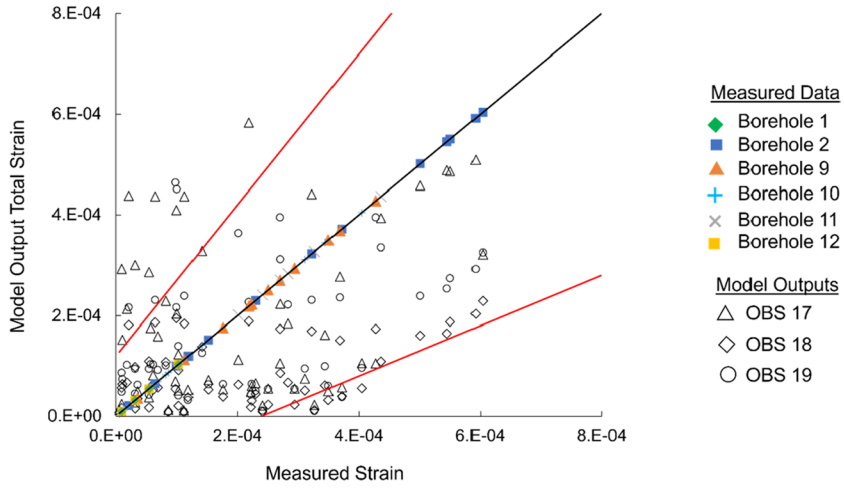

Fig. 13 Calibrated model outputs relative to measured field data

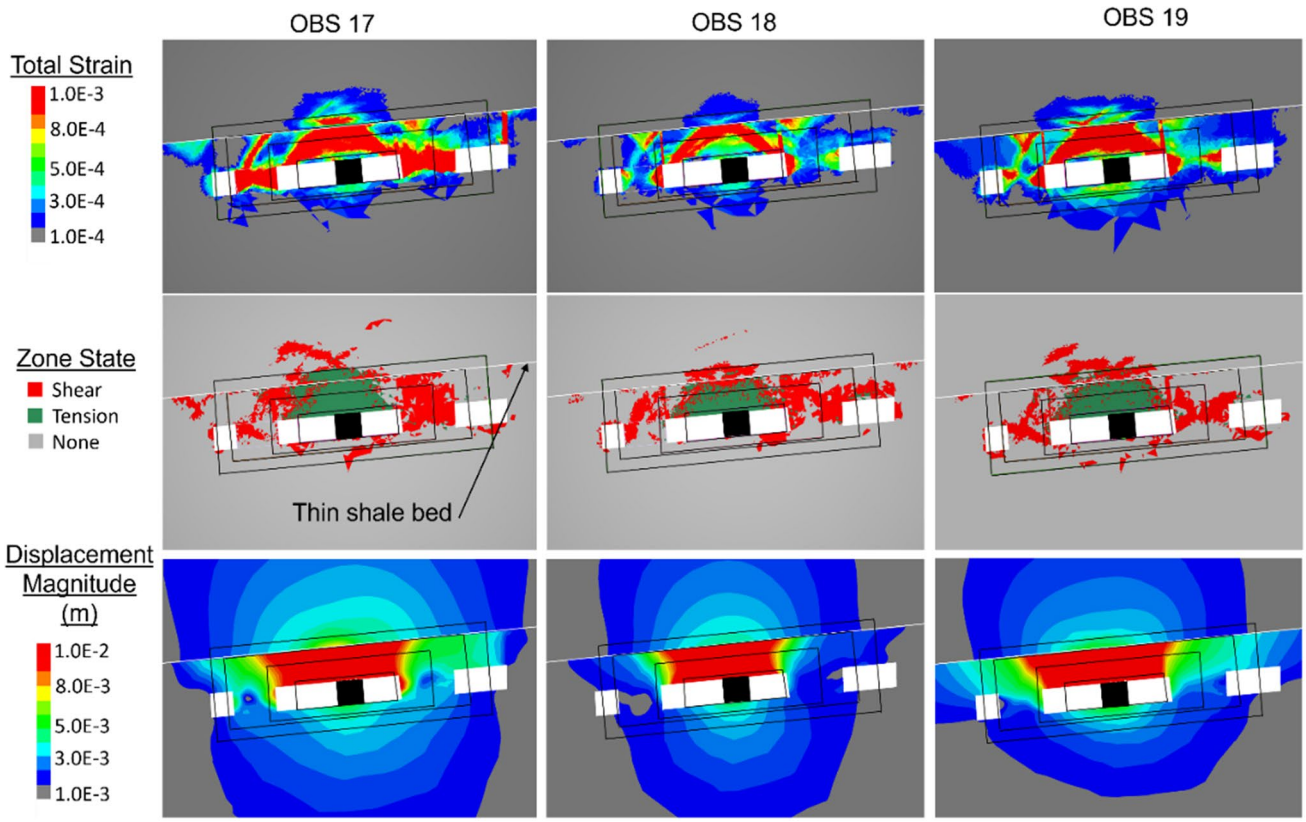

Fig. 14 Total strain, failure state, and displacement magnitude plots for the calibrated range of model inputs. Black rectangles indicate the location of damage zones, while the central black square represents the location of a removed pillar

Discussion

The calibrated models range in accuracy from 78.2 to 89.1% within the 50% tolerance interval. It should be noted that no single model was capable of producing accurate results over the entire range of measured strain values. For instance, models that perform with good correlation at higher strain values tend to over-predict the lower measured strains and vice-versa. Various combinations of GSI and damage zone extents can result in similar, non-unique outcomes, and higher densities of installed sensors may aid in the further localization/validation of damage extents. The orientation of the maximum horizontal stresses was found to result in little change in the model accuracy with respect to the measured data. One explanation for this

could be that the majority of measurement boreholes are installed near vertically and are most sensitive to changes in the axial direction. It is recommended for future deployments to include angled measurement boreholes in multiple directions around the same location such that deformation attributable to horizontal stresses can be identified. The calibration conducted in this study involves the comparison of measured strain collected from the field with a model constructed with a generalized geometry of the site geology and mine excavations. Despite efforts to constrain errors in the development of the model geometry, uncertainty still exists. Efforts to address uncertainty in the geometry development include enhanced diamond drilling for geologic unit identification and sample procurement and LiDAR scanning for more realistic excavation shapes. As the strains noted in the model can be highly localized around the stoping area, the model is sensitive to the location of the measurement sites from which strain profiles are collected for comparison with field results.

Rock mass damage due to excavation in development headings was assumed to have a minimal impact on model calibration. This assumption was derived from the low-measured strains close to the excavation boundary during monitoring after the pillar extraction. In addition, field observations such as borescope data and visual inspections indicate minimal blast fracturing beyond 10 cm into the rock mass. Further investigation is required to validate this assumption.

The use of the Taguchi method allowed for the rapid identification of controlling parameters which have outsized the influence on model calibration. When using inputs that may have a much greater influence on model responses than others, it is recommended to identify these parameters first, such that they can be isolated, and the Taguchi design of experiment is used to experiment on less influential parameters.

The presented study demonstrates how DOFS measurements from a field scale instrumentation study could be used to produce a calibrated mine-scale numerical model. It is important to note, however, that model calibration is a part of a design-execute-monitor-calibrate loop. Further studies that utilize the calibrated model to perform predictive analysis and follow up with monitoring of the execution phase of the mining cycle should be performed to assess the applicability of the conducted calibration.

Conclusions

Numerical model calibration is a critical step in the design process for underground structures such as caverns, mine excavations, and bulk-mining zones. The ability to monitor large underground excavations with DOFS presents a unique opportunity for the calibration of mine-scale numerical models.

In this work, the dataset generated from DOFS using a novel HOFC designed for distributed strain sensing in brittle media and grouted boreholes was employed for the calibration of a mine-scale numerical simulation of a room and pillar extraction operation in a competent rock mass.

The calibration process was conducted using a combination of Taguchi experimental design for the initial investigation of rock mass properties and those associated with a thin shale bedding plane in the immediate roof section. Comparison of measured strain values from the HOFC with numerical model outputs of the total strain values in models with no rock mass damage assigned allowed for the identification of the extent of a blast damage zone, which was used to inform the degradation of rock mass properties in subsequent models.

Stress conditions in the tectonically complex historic mining area were analyzed by changing the direction and magnitude of horizontal stresses applied to the model. It was noted that several combinations of GSI and modeled stresses could be used to develop a range of model inputs which result in acceptable outputs with respect to field data measured after pillar extraction.

Calibration of interface properties designed to simulate the thin shale bed yielded little information, indicating that a higher sensor density in the field or laboratory-scale testing of the geologic contact may be required to further constrain the ranges of assigned properties.

Model calibration resulted in the identification of GSI ranges for the mining area between 65 and 70, depending on in situ stresses applied to the model. The calibrated model presented in this work may prove useful for forward analysis of various mining scenarios, such as pillar extraction sequences, support designs, and the identification of potential damage to critical mine infrastructure. Further monitoring studies in similar mining areas will provide insights into the ability of the calibrated model for forward analysis.

Author contribution Conceptualization: SN, TS, ME, PB. Sensor installation: SN, TS, PB, DG. Data analysis: SN, DG, KK. Manuscript preparation: SN, TS, ME, DG, KK, PB.

Funding This research is funded by the National Institute of Safety and Health (NIOSH) under contract 75D30120C09233.

Data availability The datasets generated during and/or analyzed during the current study are available from the corresponding author on reasonable request.

Declarations

Ethics approval Not applicable.

Consent to publish All authors agree to publication in the journal.

Conflict of interest The authors declare no competing interests.

References

Andrieux PP, Hudyma MR, O'Connor CP, Li H, Cotesta L, Brummer RK (2008) Calibration of large-scale three-dimensional non-linear numerical models of underground mines using microseismic data. In Proceedings of the First International FLAC/DEM Symposium, Minneapolis, pp 25–27

ASTM Standard (2014) D7012-14e1 *Standard test methods for compressive strength and elastic moduli of intact rock core specimens under varying states of stress and temperatures*. ASTM International, West Conshohocken, USA.

ASTM Standard (2016) D3967-16 Standard test method for splitting tensile strength of intact rock core specimens". ASTM International, West Conshohocken, USA.

Bahrani N, Hadjigeorgiou J (2018) Influence of Stope Excavation on Drift Convergence and Support Behavior: Insights from 3D Continuum and Discontinuum Models. Rock Mech Rock Eng 51:2395–2413. https://doi.org/10.1007/s00603-018-1482-5

Bowersox JR, Greb S, Zhu J, Harris D (2021) Geomechanical properties will constrain CO2 injection into the lower Ordovician Rose Run sandstone deep saline reservoir, Appalachian Basin, Kentucky, USA. J Rock Mech Geotech Eng 13(5):947–960

Cordova D, Zingano A, Gonçalves I (2022) Unplanned dilution back analysis in an underground mine using numerical models. REM Int Eng J 75(04). https://doi.org/10.1590/0370-44672021750093

Esterhuizen E, Mark C, Murphy MM (2010) Numerical model calibration for simulating coal pillars, gob and overburden response. In: Proceedings of the 29th international conference on ground control in mining. West Virginia University Morgantown

Gholamzadeh B, Nabovati H (2008) Fiber optic sensors. Int J Electron Commun Eng 2(6):1107–1117

Guan Z, Jiang XZ, Wu YB, Pang ZY (2015) Study on monitoring and early warning of karst collapse based on BOTDR technique. NCKRI Symposium 5, 14th Sinkhole Conference, pp. 408–414

Hoek E (1994) Strength of rock and rock masses. ISRM News J 2:4–16

Hoek E, Brown ET (2019) The Hoek–Brown failure criterion and GSI – 2018 edition. J Rock Mech Geotech Eng 11(3):445–463. https://doi.org/10.1016/j.jrmge.2018.08.001. (**ISSN 1674-7755**)

Jones E, Beck D, Reusch F (2016) The use of underground laser mapping for numerical model calibration. In ISRM EUROCK (pp. ISRM-EUROCK). ISRM

Kellaway M, Taylor D, Keyter GJ, Venture BCJ (2012) The use of geotechnical instrumentation to monitor ground displacements during excavation of the ingula power caverns, for model calibration and design verification purposes. Tech. rep, The Southern African Institute of Mining and Metallurgy

Kim B-H, Larson MK, Lawson HE (2018) Applying robust design to study the effects of stratigraphic characteristics on brittle failure and bump potential in a coal mine. Int J Min Sci Technol 28(1):137–144

Levandowski W, Hermann R, Briggs R, Boyd O, Gold R (2018) An updated stress map of the continental United States reveals heterogeneous intraplate stress. Nat Geosci 11(6):433–437. https://doi.org/10.5066/P9BA1104,USGSEarthquakeHazardsProgram

Moffat RA, Beltran JF, Herrera R (2015) Applications of BOTDR fiber optics to the monitoring of underground structures. Geomech Eng 9(3):397–414. https://doi.org/10.12989/gae.2015.9.3.397

Nowak S, Sherizadeh T, Esmaeelpour M, Guner D, Karadeniz K (2022) Hybrid fiber optic cable for strain profiling and crack growth measurement in rock, cement, and brittle installation media. Sensors 22(24):9685

Rafiei Renani H, Martin CD, Hudson R (2016) Back analysis of rock mass displacements around a deep shaft using two- and three-dimensional continuum modeling. Rock Mech Rock Eng 49:1313–1327. https://doi.org/10.1007/s00603-015-0831-x

RocScience (2023) *Generalized Hoek-Brown criterion*. RSData Documentation. https://www.rocscience.com/help/rsdata/documentation/materials/strength-criterion/generalized-hoek-brown-criterion, accessed 2023

Seabrook BC, Ellmauthaler A, LeBlanc M, Jaaskelainen M, Maida JL, Wilson GA (2022) Comparison of Raman, Brillouin, and Rayleigh Distributed Temperature Measurements in High-Rate Wells. Petrophysics 63(06):685–699

Shapka-Fels T, Elmo D (2022) Numerical modelling challenges in rock engineering with special consideration of open pit to underground mine interaction. Geosciences 12(5):199. https://doi.org/10.3390/geosciences12050199

Taguchi G, Phadke MS (1984). Quality engineering through design optimization, Ch. 5, In: Quality control, robust design, and the Taguchi method, ed. by Dehnad K, Pacific Grove, CA: Wadsworth & Brooks/Cole Advanced Books & Software, pp. 77–96

Walton G, Sinha S (2022) Challenges associated with numerical back analysis in rock mechanics. J Rock Mech Geotech Eng 14(6):2058–2071. https://doi.org/10.1016/j.jrmge.2022.01.010

Walton G, Diederichs M, Punkkinen A, Whitmore J (2016) *Back analysis of a pillar monitoring experiment at 2.4km depth in the Sudbury Basin* Canada. Int J Rock Mech Min Sci 85:33–51. https://doi.org/10.1016/j.ijrmms.2016.03.001. (**ISSN 1365-1609**)

Woo K-S, Eberhardt E, Rabus B, Stead D, Vyazmensky A (2012) Integration of field characterisation, mine production and InSAR monitoring data to constrain and calibrate 3-D numerical modelling of block caving-induced subsidence. Int J Rock Mech Min Sci 53:166–178